5th International Conference on Experimental Fluid Mechanics ICEFM 2018 Munich
Munich, Germany, July 2-4, 2018

Simultaneous measurement of 3D velocity field and wall temperature distribution of an impinging chevron jet

Mattia Contino[1*], Carlo Salvatore Greco[1], Tommaso Astarita[1], Gennaro Cardone[1]

[1] University of Naples Federico II, Department of Industrial Engineering, Naples, Italy

[*] mattia.contino@unina.it

Abstract

Time Resolved Tomographic Particle Image Velocimetry and InfraRed thermography techniques are simultaneously applied to investigate the correlation between the passive heat and momentum transportation of a continuous jet impinging on a flat plate. A circular and a chevron nozzle exit are investigated at fixed Reynolds number and at fixed nozzle-to-plate distance. Mean and turbulent fluctuation distributions of temperature at impinging surface and of velocity close to the wall are presented. Measurements revealed low temperature and high velocity fluctuations located along the apices of the chevron nozzle.

1 Introduction

The investigation of correlation between momentum and heat transport is of peculiar importance in turbulent flows. Particularly interesting turbulent flows are the impinging jets which gained large attention because of their wide range of industrial applications (drying, cooling, tempering) and great variety of possible nozzle geometries (Ianiro and Cardone, 2012; Gutmark et al., 1985). The specific cooling efficiency issue strictly depends on how much the flow is able to develop a turbulent flow in proximity of the wall (Gardon and Akfirat, 1965). Turbulent flows are characterised by strongly three-dimensional and unsteady behaviour and they are characterized by a wide range of length and time scales (Kolmogorov, 1941). Hence, it is of main interest to understand the unsteady behaviour of the flow and the thermal fluctuations in proximity of the impinged wall.

The most promising non-invasive techniques which allows to investigate unsteady complex flows from velocity and thermal points of view are respectively the Time Resolved Tomographic Particle Image Velocimetry (TR Tomo-PIV) and High Speed InfraRed (IR) thermography. The first technique provides four dimensional (three-dimensional time-resolved) information about the flow (Westerweel et al., 2013). The other mentioned technique detects the electromagnetic energy radiated by an object and converts it into a sequence of instantaneous 2D temperature maps (Astarita and Carlomagno, 2012).

The ability to control the structure of a flow is one of the most important topics in fluid dynamics. The most attractive flow control technique involves the application of geometrical modifications to the nozzle exit (Gutmark and Grinstein, 1999; Schadow et al., 2004). A specific nozzle geometry, the chevron nozzle, has been investigated in supersonic applications by NASA in order to reduce noise emission without affecting trust (Bridges and Brown, 2004). Subsonic applications of this nozzle exit were examined to answer whether such a nozzle geometry could produce significant enhancement to heat transfer capabilities and mixing properties of standard circular jet (Reeder and Samimy, 1996; Violato et al., 2012).

Through the simultaneous application of the two mentioned techniques the present paper will describe the correlation between near-wall 3D velocity flow field and the thermal footprint of a circular and a six-chevron cold jet impinging from above on a flat horizontal plate placed in a tank filled with hot water.

2 Experimental apparatus and procedure

The experimental apparatus is described in the following. A schematic is reported in figure 1. The water facility includes two tanks: a small one filled with cold water (293K) and a big one filled with hot water (298K). Both tanks are controlled in temperature with accuracy of 0.03K. A nozzle (N) (circular or chevron) of diameter D = 10mm is suspended at a fixed distance from wall (H/D=2) over a circular sapphire window (S) (diameter 150mm, thickness 4mm) sealed on the bottom of the hot tank. On the other side of the window are positioned 4 high speed PIV cameras (C_i) and a Mid-Wavelength InfraRed (MWIR) camera (T_1) which share a common trigger. The test starts when the geared pump (P) pushes the cold water through a flow meter (F). The fluid finally exhausts through the nozzle at a constant mass rate equal to 240L/h resulting in a Reynolds number equal to 8100. After 120 seconds the pump is working, the simultaneous Tomo-Thermographic acquisition starts.

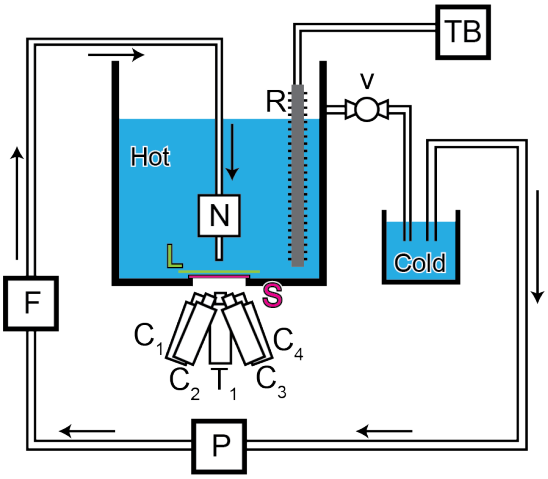

Figure 1: Scheme of the experimental apparatus. P) Gear type pump; F) Flowmeter; N) Nozzle (circular or chevron); L) Laser volume; S) Sapphire window; TB) Thermal Bath; R) Radiator; V) Valve; C_i) High Speed PIV cameras; T_1) High Speed IR camera.

The temperature difference is monitored by two RTDs Pt100 (1/10 DIN) each of which placed in one of the two tanks. Initially the valve (V) is opened and the thermal bath cools down the entire loop through a radiator placed in the larger tank. Once the lower temperature is reached, the pump is stopped and the valve is closed. Then the fluid in the larger tank is warmed up changing the temperature target of the thermal bath. The choice to manage with such small temperature difference of about $\Delta T = 5$K is justified by the non-linear behaviour of water density depending on its temperature. With such described conditions, the water will change its density only of 0.1% passing through the lower temperature to the higher one. As a matter, it can be assumed that small temperature differences do not govern fluid motion. Hence, such kind of contaminant has no dynamical effect on the fluid motion itself. For this reason the temperature difference can be fairly used as additional tracer in the flow under investigation (Warhaft, 2000).

The developed set up is based on the property of water to absorb radiation at sub-millimetre scale while it is perfectly transparent in the laser wavelength range. Hence, this makes possible to measure non-isothermal instantaneous turbulent fluctuations of the fluid in the boundary layer through an IR-transparent window. The most appropriate material for water submerged applications is sapphire. In addition, Anti-Reflective coating is applied on one side of the window.

The round nozzle of exit diameter D = 10mm and contraction ratio of 56.25 has been characterized in (Violato and Scarano, 2011). A six-chevrons exit is applied on top of the circular nozzle profile, with tabs inclined towards the jet axis. The chevron length ℓ is 0.43D and the penetration depth p is 0.134D, according to the model SMC006 used by (Bridges and Brown, 2004). A schematic of the chevron nozzle is shown in figure 2.

Neutrally buoyant LaVision Polyamide High Quality particles of 56µm of diameter are employed to uniformly seed the water. The illumination is provided by a solid-state diode-pumped LDY303 Nd:YLF laser (2×20mJ). The light scattered by the particles is recorded by a tomographic system composed of four Speed Sense M110 (sensor dimensions 1280×800 pixels, pixel pitch 20µm) CMOS cameras arranged

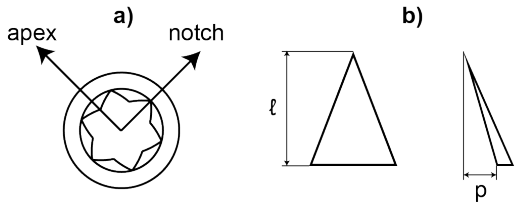

Figure 2: a) Azimuthal position of chevron notch and apex; b) details of the chevron nozzle: length ℓ and penetration depth p.

vertically below the hot tank in a cross-like configuration. Tokina AT-X M100 PRO D objectives of 100mm focal length are set with a numerical aperture $f_{\#} = 32$ to allow focused imaging of the illuminated particles. The resulting field of view is 5.1D $\times$ 3D with a digital resolution of 21.5 pixels/mm. Sequences of images of tracer particles are recorded at 1600Hz. A total of 3400 images are acquired for a total time of acquisition of 2.125s.

A CEDIP JADE III (Mid Wave) IR camera working in the $3-5$µm band is employed to measure the temperature fluctuations through the sapphire window with a spatial resolution of 2.16 pixels/mm. The camera sensor has nominal dimensions of 320×240, pixel pitch of 30µm, temperature sensitivity of 0.025K. For the current application the sensor is used as cropped to 160×120 pixels to achieve higher frequency of acquisition. The resulting field of view is 7.3D $\times$ 5.5D. Images are acquired at frequency of 400Hz and Integration Time (IT) equal to 1100µs. A total of 34,000 samples are acquired starting from the trigger resulting in a time of acquisition of 85s.

3 Results

Velocity magnitude and the Turbulent Kinetic Energy (TKE) are the main actors which mainly influences the heat exchange and mixing. These velocity quantities will be respectively compared to mean and standard deviation temperature maps. The tests are carried out with a constant mass flow rate equal to 240L/h resulting in a Reynolds number of 8100. The nozzle exit is positioned above the sapphire window at H/D=2. The acquisition frequency of velocity system is set to 1600Hz. On the other side, the temperature system acquisition frequency is 400Hz with IT = 1100µs. It has to be noted that the two measures investigate the flow at different location along the nozzle to plate direction. The InfraRed thermography measurements are relative to the wall closest sub-millimetre boundary water layer while the first plane of the Time Resolved Tomo-PIV measurements is placed 0.173D over the wall.

The results described in (Violato et al., 2012) will be taken as reference in the following discussion where thermal contours will be presented overlapped on velocity coloured maps.

3.1 Circular nozzle exit

The interaction of the circular jet with the impinged wall is reported in figure 3. In figure 3(a) a contour of the mean temperature map is superimposed over the total velocity magnitude normalized to the average bulk velocity W_0. The mean temperature pattern appears to be perfectly axisymmetric with respect to the impingement centre. On the other hand, the mean velocity contour perfectly imitates the circular temperature pattern. A minimum of velocity magnitude is located on the impingement. Moving away from the centre a maximum is visible at about 0.75D.

In Figure 3(b) the standard deviation temperature contour is superimposed over the TKE map. The standard deviation of temperature contours are explanatory to spot the high mixing regions and the potential core region. As a matter, the region in proximity of the impingement centre shows temperature fluctuations of less than 0.05K until 1.25D. At the specific location of 1.75D there is the presence of the maximum temperature fluctuations (Violato et al., 2012). Beyond that location, the temperature fluctuations weakly reduce along the development of the wall jet region. From the velocity point of view, the jet is characterized by a local minimum of TKE in the stagnation region which extends to 0.75D. Then the fluctuations rapidly increase until reaching a local maximum in proximity of 1D of distance from the impact point. A second local maximum of the TKE is located further away from the impingement point (1.75D). Then the velocity fluctuations are characterised by a slow decaying.

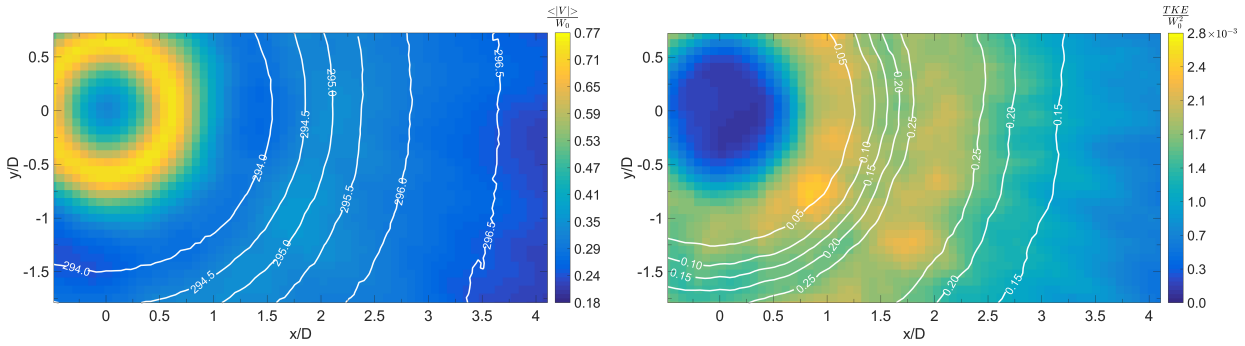

(a) White contour) Mean temperature; coloured map) Normalized total velocity magnitude.

(b) White contour) Standard deviation temperature; coloured map) Normalized TKE.

Figure 3: Mean and fluctuations quantities for the circular nozzle.

In figure 4 a three-dimensional representation of the circular jet case as isosurface plots of different quantities is shown. The isosurface in red color corresponds to the axial velocity surface corresponding to the value $w/W_0 = 0.53$. This can be associated with good approximation with the potential core impinging on the plate. In green color the normalized TKE corresponding to the value $1.535 \cdot 10^{-3}$ is pictured. The TKE blanket spreads from the core jet with an evident ripple placed at distance of 1.75D. As background of the 3D frame it is represented the mean temperature map. The red dashed line represents the projection of PIV volume over the thermal map.

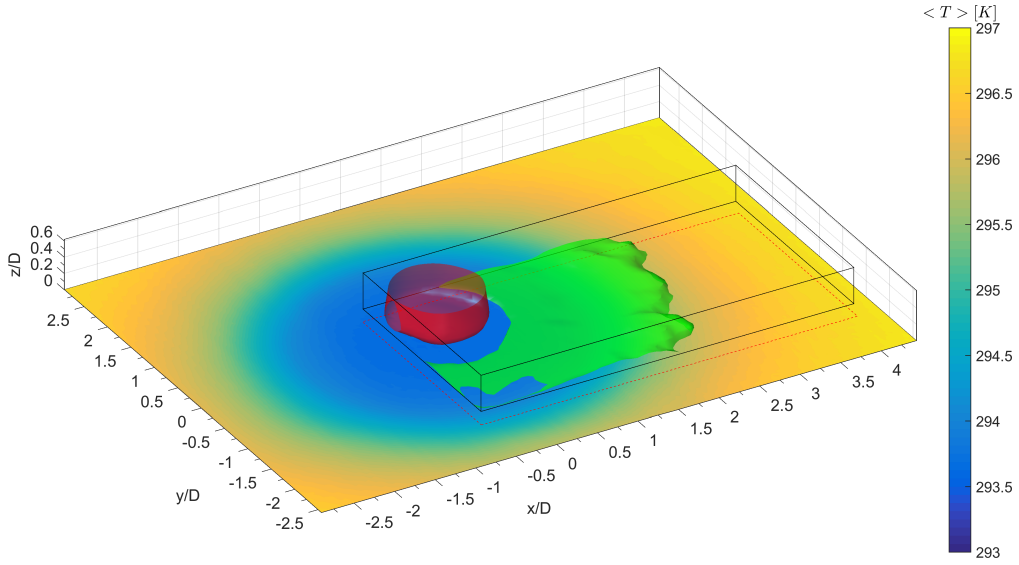

Figure 4: (Circular nozzle) isosurface of axial velocity $w/W_0 = 0.53$ (in red), isosurface of $TKE/W_0^2 = 1.535 \cdot 10^{-3}$ (in green), mean temperature map on the background (colorbar on the right).

3.2 Chevron nozzle exit

Figure 5 is representative to describe the interaction of the chevron jet with the impinged wall. The figure 5(a) presents the contour of the mean temperature map overlapped to the normalized total velocity magnitude map. A noticeable common point with the circular case exists, that is the presence of minimum of total velocity magnitude in proximity of the central region of impingement. On the other hand, this region is surrounded by a circular region of maximum velocity located at 0.5D. A six-point-star shape characterises both the temperature and velocity distributions. This is due to the flow clearly issued from the nozzle

custom shape. Comparing the velocity profiles, the potential core of the chevron jet has a thinner cross-section with respect to the circular case. In addition, the chevron jet is characterised by higher value of total velocity magnitude. The alternating pattern of high and low total velocity shows that the higher values of velocity are measured along the directions corresponding to the apices of the nozzle. This behaviour could be ascribed to the fact that the jet experiences an axis-switching like behaviour on the wall, as characteristic for cross-shaped continuous jets (Rau et al., 2014; Chen and Yu, 2014; Violato et al., 2012). The temperature map shows the characteristic six-point-star shape which accurately resembles the nozzle exit shape similarly to what observed for the flow field.

Figure 5(b) describes the standard deviation temperature contour superimposed over the velocity TKE map. As first, it can be noticed that the lowest temperature and the highest velocity fluctuations values are measured along apices' directions. This behaviour switches along the notches' directions.

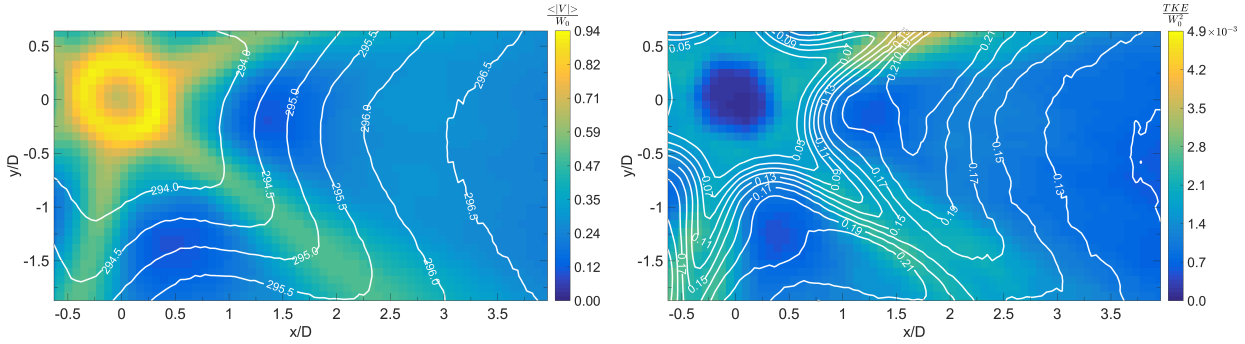

(a) White contour) Mean temperature; coloured map) Normalized total velocity magnitude.

(b) White contour) Standard deviation temperature; coloured map) Normalized TKE.

Figure 5: Mean and fluctuations quantities for the chevron nozzle.

In figure 6 there is reported a three-dimensional representation of the chevron jet case. Like in the circular case, the red isosurface corresponds to the value $w/W_0 = 0.53$ while in green color there is the normalized TKE corresponding to the value $1.535 \cdot 10^{-3}$. As background of the 3D frame it is represented the mean temperature map. The red dashed line represents the projection of PIV volume over the thermal map. The remarkable difference from the circular one is the six-shaped TKE pattern departing from the core jet.

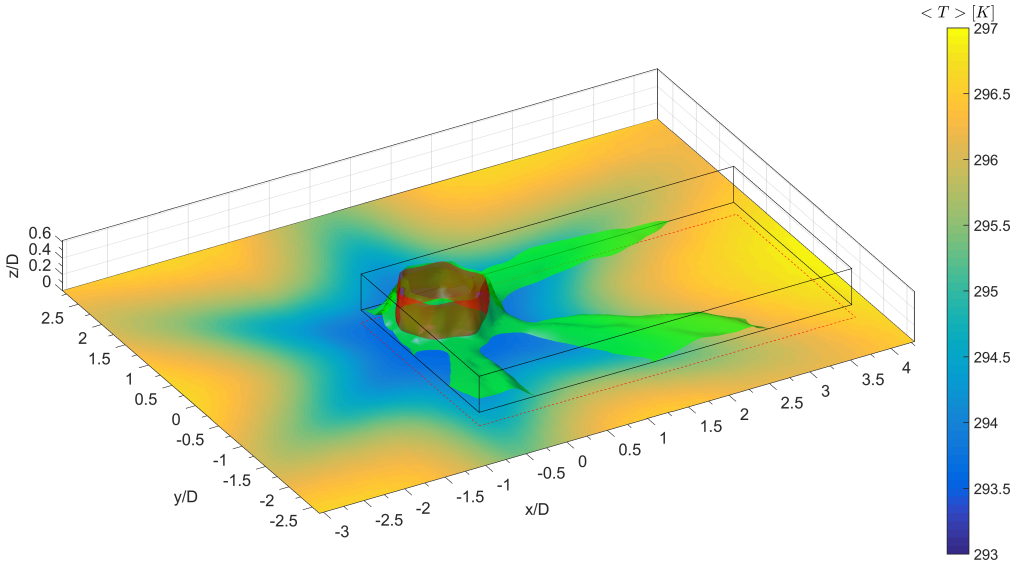

Figure 6: (Chevron nozzle) isosurface of axial velocity $w/W_0 = 0.53$ (in red), isosurface of $TKE/W_0^2 = 1.535 \cdot 10^{-3}$ (in green), mean temperature map on the background (colorbar on the right).

4 Conclusion

In the present paper an impinging chevron jet is experimentally investigated at Reynolds number equal to 8100 and compared with a circular jet at the same flow regime. Velocity measurements are carried out through Time Resolved Tomograhpic Particle Image Velocimetry technique. Simultaneously, 2D temperature maps are acquired by InfraRed thermography technique. The nozzle to plate distance is fixed at H/D=2 in both cases. The jet exhausts in a tank at small temperature difference from the jet itself ($\Delta T = 5$K). According to average velocity profiles, the potential core of the chevron jet has a thinner cross-section with respect to the circular case. This can be justified by the higher velocity in the impingement centre in the chevron case. Regions of higher total velocity magnitude in correspondence to the chevron apices are noticeable. In addition, a star-shaped pattern is clearly distinguishable. The average temperature maps accurately follow the velocity pattern. In the circular case, the second radial peak placed at 1.75D from the impingement centre is clearly highlighted in temperature maps. The lowest temperature and the highest velocity fluctuations values are concentrated along apices' directions for the chevron nozzle.

References

Astarita T and Carlomagno GM (2012) *Infrared thermography for thermo-fluid-dynamics*. Springer Science & Business Media

Bridges J and Brown C (2004) Parametric testing of chevrons on single flow hot jets. in *10th AIAA/CEAS Aeroacoustics Conference*. page 2824

Chen N and Yu H (2014) Mechanism of axis switching in low aspect-ratio rectangular jets. *Computers & Mathematics with Applications* 67:437–444

Gardon R and Akfirat JC (1965) The role of turbulence in determining the heat-transfer characteristics of impinging jets. *International journal of heat and mass transfer* 8:1261–1272

Gutmark E and Grinstein F (1999) Flow control with noncircular jets. *Annual review of fluid mechanics* 31:239–272

Gutmark E, Schadow K, Parr D, Harris C, and Wilson K (1985) The mean and turbulent structure of noncircular jets. in *1985 AIAA Shear Flow Control Conference*

Ianiro A and Cardone G (2012) Heat transfer rate and uniformity in multichannel swirling impinging jets. *Applied Thermal Engineering* 49:89–98

Kolmogorov AN (1941) The local structure of turbulence in incompressible viscous fluid for very large reynolds numbers. in *Dokl. Akad. Nauk SSSR*. volume 30. pages 299–303

Rau MJ, Dede EM, and Garimella SV (2014) Local single-and two-phase heat transfer from an impinging cross-shaped jet. *International Journal of Heat and Mass Transfer* 79:432–436

Reeder M and Samimy M (1996) The evolution of a jet with vortex-generating tabs: real-time visualization and quantitative measurements. *Journal of Fluid Mechanics* 311:73–118

Schadow K, Gutmark E, Parr D, and Wilson K (2004) Selective control of flow coherence in triangular jets. *Experiments in Fluids* 6:129–135

Violato D, Ianiro A, Cardone G, and Scarano F (2012) Three-dimensional vortex dynamics and convective heat transfer in circular and chevron impinging jets. *International Journal of Heat and Fluid Flow* 37:22–36

Violato D and Scarano F (2011) Three-dimensional evolution of flow structures in transitional circular and chevron jets. *Physics of Fluids* 23:124104

Warhaft Z (2000) Passive scalars in turbulent flows. *Annual Review of Fluid Mechanics* 32:203–240

Westerweel J, Elsinga GE, and Adrian RJ (2013) Particle image velocimetry for complex and turbulent flows. *Annual Review of Fluid Mechanics* 45:409–436